JOC The Journal of Organic Chemistry

Article

pubs.acs.org/joc

A DFT Study of the [3 + 2] versus [4 + 2] Cycloaddition Reactions of 1,5,6-Trimethylpyrazinium-3-olate with Methyl Methacrylate

Luis R. Domingo,*[,†] Jose A. Sáez,[‡] John A. Joule,[§] Lydia Rhyman,[∥] and Ponnadurai Ramasami[∥]

[†]Departamento de Química Orgánica, Universidad de Valencia, Dr. Moliner 50, 46100 Burjassot, Valencia, Spain

[‡]Instituto de Tecnología Química, UPV-CSIC, Camino de Vera s/n, 46022 Valencia, Spain

[§]The School of Chemistry, The University of Manchester, Manchester M13 9PL, U. K.

[∥]Computational Chemistry Group, Department of Chemistry, Faculty of Science, University of Mauritius, Réduit, Mauritius

Supporting Information

ABSTRACT: The reaction between 1,5,6-trimethylpyrazinium-3-olate and methyl methacrylate (MMA) yielding a lactone−lactam has been studied using the DFT method at the B3LYP/6-31G(d) level. It is concluded that formation of the lactone−lactam is a domino process involving three consecutive reactions: (i) a 1,3-dipolar cycloaddition (13DC) reaction between the pyrazinium-3-olate and MMA yielding a [3 + 2] cycloadduct (CA); (ii) a skeletal rearrangement, which converts the [3 + 2] CA into a formal [4 + 2] CA, possessing a diazabicyclo[2.2.2]octane structure; and finally, (iii) an S_N2 reaction, promoted by halide anion, with concomitant nucleophilic attack of the created carboxylate anion on an iminium carbon with formation of the lactone ring present in the lactone−lactam. Analysis of the four competitive channels associated with the 13DC reaction indicates that this cycloaddition takes place with complete *endo* stereoselectivity and *6* regioselectivity, yielding [3 + 2] CA. The subsequent skeletal rearrangement also takes place in an elementary step via a non-concerted mechanism. Electron localization function bonding analysis makes it possible to establish that the bicyclo[2.2.2]octane skeleton present in the lactone−lactam complex structure is not attained via a Diels−Alder reaction between pyrazinium-3-olate and MMA.

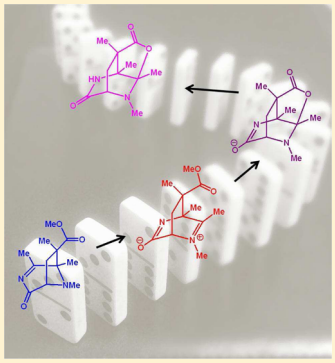

INTRODUCTION

The 1,3-dipolar cycloaddition (13DC) reaction is an effective route for the synthesis of five-membered heterocyclic structures.[1] The ring systems arising from 13DC reactions are the backbones of some natural products.[2] Nitrogen-containing heterocycles occur widely in nature, in isolation and as structural subunits in various families of alkaloids with laboratory,[3] industrial, and pharmacological applications.[4]

Following and inspired by the pioneering studies of Katritzky et al. on pyridinium-3-olates,[5] some of us have been particularly interested in the cycloaddition reactions of pyrazinium-3-olates[6,7] as a means for the construction of complex structures.

Thus, the cycloadditions of a range of substituted 5-methylpyrazinium-3-olates **1** with unsymmetrical dipolarophiles such as methyl acrylate (MA) **2** have been studied experimentally (see Scheme 1).[6] These reactions produced 2-oxo-3,8-diazabicyclo[3.2.1]octane-6-carboxylates **4**, via imine/enamine tautomerism of presumed, non-isolated 13DC adducts **3**.

The reaction of pyrazinium-3-olate **1a** ($R^1 = R^2 = R^3 = Me$) with the more hindered dipolarophile methyl methacrylate (MMA) **5** yielded a more complex structure **8**, which was characterized by X-ray crystallography (see Scheme 2).[7] Noting that **8** possesses a diazabicyclo[2.2.2]octane skeleton, it was suggested that this could have been reached via an initial Diels−Alder (DA) reaction, involving the azadiene unit in **1a**, to initially yield diazabicyclo[2.2.2]octane adduct **6**.[7] An intramolecular interaction between the ester carbonyl group and the iminium cation present in **6** would provide **7**, which by N-protonation and hydrolysis (or demethylation) of the MeO^+═C unit would then finally afford the observed tricyclic lactone−lactam **8**.

On the basis of this result, it was speculated[7] that the [3 + 2] cycloadduct (CA) pyrazinium-3-olate products previously obtained[6] might actually derive via rearrangement of initial [4 + 2] CA adducts and that the initial adduct had, in this special case, been trapped by intramolecular interaction with the ester. Indeed, this also called into question the comparable [3 + 2] CAs obtained in Katritzky's work on pyridinium-3-olates. Could these also derive from rearrangement of initial [4 + 2] CAs?

The 13DC reactions shown in Scheme 1 have recently been theoretically studied using the density functional theory (DFT) method.[8] These studies indicated that these cycloaddition reactions take place via a one-step mechanism through highly asynchronous transition state structures (TSs) associated with the most favorable nucleophilic/electrophilic interactions between either the C2 or C6 carbon of 5-methylpyrazinium-3-olates **1** and the β conjugated position of MA **2**.

Received: December 17, 2012
Published: January 23, 2013

Scheme 1. 13DCs of Substituted Pyrazinium-3-olates 1 with MA 2

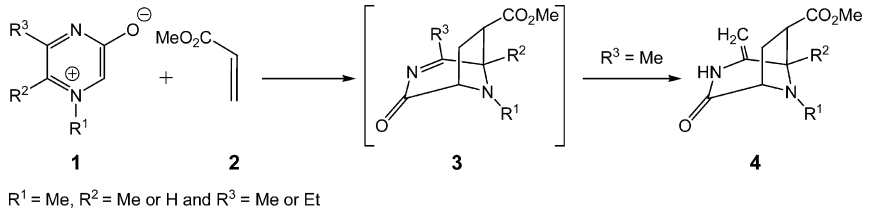

R^1 = Me, R^2 = Me or H and R^3 = Me or Et

Scheme 2. Proposed Mechanism for the Cycloaddition of 1a with MMA 5

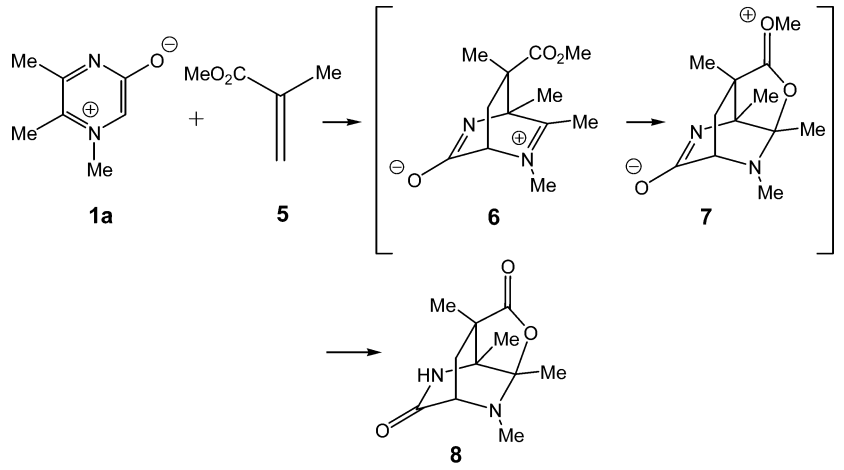

Herein, we present a theoretical study for the reaction between pyrazinium-3-olate **1a** and MMA **5** yielding lactone–lactam **8** shown in Scheme 2. The cardinal objective of this paper is to shed light on the mechanism of the formation of the diazabicyclo[2.2.2]octane skeleton present in **8**. Within this objective, we address the fundamental question of whether **8** is formed by a [4 + 2] cycloaddition reaction such as proposed earlier as in Scheme 2 or by a [3 + 2] cycloaddition such as that given by MA **2**, followed by a skeletal rearrangement to yield **6**. Additionally, the formation of the lactone ring present in lactone–lactam **8** is also studied.

COMPUTATIONAL METHODS

DFT computations were carried out using the B3LYP[9] exchange-correlation functionals, together with the standard 6-31G(d) basis set.[10] The optimizations were carried out using the Berny analytical gradient optimization method.[11] In order to test the reliability of this basis set, the stationary points involved in the formation of lactone–lactam enolate **13** were optimized using the 6-311G(d) basis set. The stationary points were characterized by frequency computations in order to verify that TSs have one and only one imaginary frequency. The intrinsic reaction coordinate (IRC) paths[12] were traced in order to check the energy profiles connecting each TS to the two associated minima of the proposed mechanism using the second order González–Schlegel integration method.[13] The electronic structures of stationary points were analyzed by the natural bond orbital (NBO) method[14] and by the electron localization function (ELF) topological analysis, $\eta(\mathbf{r})$.[15] The ELF study was performed with the TopMod program[16] using the corresponding monodeterminantal wave functions of the selected structures of the IRC. All computations were carried out with the Gaussian 09 suite of programs.[17]

The global electrophilicity index, ω, is given by the following expression,[18] $\omega = (\mu^2/2\eta)$, in terms of the electronic chemical potential μ and the chemical hardness η. Both quantities may be approached in terms of the one-electron energies of the frontier molecular orbitals HOMO and LUMO, ε_H and ε_L, as $\mu \approx (\varepsilon_H + \varepsilon_L)/2$ and $\eta \approx (\varepsilon_l + \varepsilon_h)$, respectively.[19] Recently, we introduced an empirical (relative) nucleophilicity index,[20] N, based on the HOMO energies obtained within the Kohn–Sham scheme[21] and defined as $N = E_{HOMO}(Nu) - E_{HOMO}(TCE)$. The nucleophilicity is referred to tetracyanoethylene (TCE) because it presents the lowest HOMO energy in a large series of molecules already investigated in the context of polar cycloadditions. This choice allows us to handle conveniently a nucleophilicity scale of positive values. The local electrophilicity indices,[22] ω_k, and the local nucleophilicity indices,[23] N_k, were evaluated using the following expressions:[24] $\omega_k = \omega P_k^+$ and $N_k = NP_k^-$, where P_k^+ and P_k^- are the electrophilic and nucleophilic Parr functions,[24] respectively, obtained through the analysis of the Mulliken atomic spin density of the radical anion and the radical cation.[24]

RESULTS AND DISCUSSION

This theoretical study was divided into three different parts: (i) analysis of the cycloaddition reaction based on DFT reactivity indices; (ii) mechanistic study of the domino reaction of pyrazinium-3-olate **1a** with MMA **5** with formation of lactone–lactam **8**; and finally (iii) an ELF bonding analysis along the formation of the most favorable [3 + 2] CA **9**, and its isomerization to formal [4 + 2] CA **6**.

1. Analysis Based on the Reactivity Indices at the Ground State of Reagents. Recent studies devoted to DA and 13DC reactions have shown that the analysis of the global and local indices defined within the context of the conceptual DFT[25] are a powerful tool to understand the reactivity in polar cycloadditions. In Table 1, the static global properties, namely, electronic chemical potential μ, chemical hardness η, global electrophilicity ω, and global nucleophilicity N indices, of pyrazinium-3-olate **1a** and MMA **5** are reported, while the local electrophilicity ω_k and local nucleophilicity N_k indices are given in Figure 1.

The electronic chemical potential of MMA **5**, μ = −4.16 eV, is lower than that of pyrazinium-3-olate **1a**, μ = −3.48 eV, indicating that along a polar cycloaddition reaction path the net charge transfer (CT) will take place from the pyrazinium-3-

dx.doi.org/10.1021/jo302730q | J. Org. Chem. 2013, 78, 1621–1629

Table 1. Electronic Chemical Potential μ, Chemical Hardness η, Global Electrophilicity ω, and Global Nucleophilicity N Indices, in eV, of Pyrazinium-3-olate 1a and MMA 5

	μ	η	ω	N
1a	−3.48	3.69	1.64	3.80
MMA **5**	−4.16	6.24	1.39	1.84

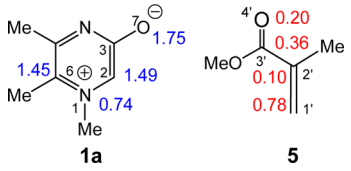

Figure 1. Local nucleophilicity of pyrazinium-3-olate **1a** (N_k in eV, blue) and local electrophilicity of MMA **5** (ω_k in eV, red).

olate **1a** toward the electron-deficient MMA **5**, in clear agreement with the CT analysis performed at the TS (see Section 2).

The electrophilicity index of pyrazinium-3-olate **1a** is 1.64 eV, a value that lies in the range of strong electrophiles on the electrophilicity scale.[26] On the other hand, pyrazinium-3-olate **1a** has a high nucleophilicity index, N = 3.80 eV, being classified as a strong nucleophile on the nucleophilicity scale.[27] MMA **5** has an electrophilicity index of ω = 1.39 eV and a nucleophilicity index of N = 1.84 eV, being classified as a moderate electrophile and as a moderate nucleophile.

In spite of the fact that pyrazinium-3-olate **1a** is slightly more electrophilic than MMA **5**, analysis of the electronic chemical potential μ indicates that the CT will take place from **1a** to MMA **5**; thus, pyrazinium-3-olate **1a** will behave as a nucleophile and MMA **5** as an electrophile. This behavior is reasonable considering the strong nucleophilic character of pyrazinium-3-olate **1a**.

Recent studies devoted to cycloaddition reactions with a polar character have shown that the analysis of the local electrophilicity index ω_k in the electrophilic component and the local nucleophilicity index N_k in the nucleophilic partner explains the observed regioselectivity. In this way, the N_k in pyrazinium-3-olate **1a** and the ω_k in MMA **5** were analyzed in order to predict the best electrophilic/nucleophilic interaction along a polar cycloaddition path and thus explain the observed regioselectivity.

MMA **5** has the largest electrophilic activation at the β conjugated C1′ position, $\omega_{C1'}$ = 0.78 eV. Note that this position is twice as electrophilically activated as the ester C3′ carbon, $\omega_{C3'}$ = 0.36 eV. On the other hand, the O7 oxygen atom and the C2 and C6 positions of the heterocyclic ring relative to the O7 oxygen are the most nucleophilically activated of pyrazinium-3-olate **1a**. The O7 oxygen atom is the most nucleophilic site of these molecules, N_{O7} = 1.75 eV, followed by the C2 position, N_{C2} = 1.49 eV, and then C6, N_{C6} = 1.45 eV.

Along a polar reaction pathway involving unsymmetrical reactants, the most favorable regioisomeric channel is that associated with the two-center interaction between the most electrophilic site of the electrophile and the most nucleophilic site of the nucleophile. Therefore, the most favorable reaction channel will be that associated with the approach of the O7 oxygen atom of **1a** toward the β conjugated C1′ position of MMA **5**. However, this reaction channel cannot progress, and consequently this interaction reversibly gives the separated reactants. On the other hand, the approach of the nucleophilic C2 position toward the β conjugated C1′ position of MMA **5** can be assisted by the concomitant ring closure with formation of the second C−C bond, to result in the formation of the final [3 + 2] or [4 + 2] CA. Note that the C6 position of pyrazinium-3-olate **1a** is also nucleophilically activated: N_{C6} = 1.45 eV. Consequently, the approach of the nucleophilic C6 position of **1a** toward the β conjugated C1 position of MMA **5** could be competitive, yielding a corresponding regioisomeric CA.

2. Mechanistic Study of the Domino Reaction of Pyrazinium-3-olate 1a with MMA 5. *2.1. Cycloaddition Reaction between Pyrazinium-3-olate **1a** and MMA **5**.* An exploration of the potential energy surface (PES) for the reaction between pyrazinium-3-olate **1a** and MMA **5** indicates that the reaction begins with the initial formation of [3 + 2] CA **9**, which experiences a skeletal rearrangement to yield formal [4 + 2] CA **6** (see Scheme 3). Because of the asymmetry of both

Scheme 3. Alternative Pathways for the 13DCs of 1a with MMA 5

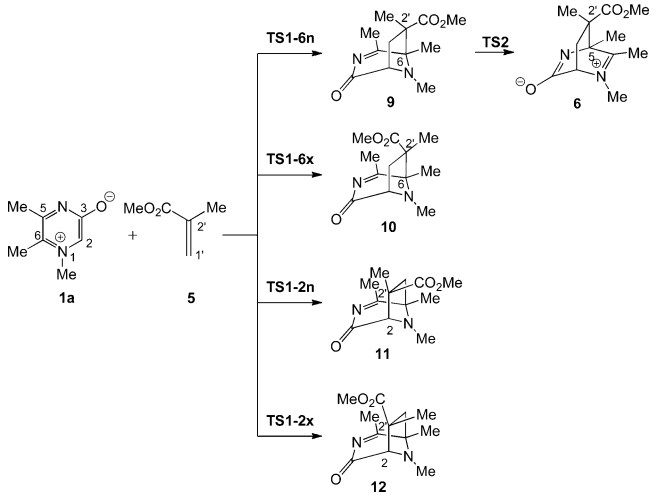

reactants, formation of four isomeric [3 + 2] CAs is feasible. They are related to the two regio- and stereoisomeric approach modes of the ester-substituted double bond of MMA **5** to the ring of **1a**. The two possible regioisomeric products are numbered 6 (C2′ linked to C6) and 2 (C2′ linked to C2), depending on the relative position of the carboxylate group in the products; the stereochemical possibilities are named *endo* and *exo* for each of these regioisomeric products. This 13DC reaction takes place through a one-step mechanism. Consequently, four TSs, **TS1−6n**, **TS1−6x**, **TS1−2n**, and **TS1−2x**, and the corresponding [3 + 2] CAs, **9**−**12**, were located and characterized. As the lactone ring present in lactone−lactam **8** must be formed via [2.2.2] bicyclic structure **6**, only the isomerization of [3.2.1] bicyclic compound **9** to **6**, via **TS2**, was studied (see Scheme 3). The total and relative energies are given in Table 2, while the geometries of the TSs are given in Figures 2 and 3.

The gas phase activation energies associated with the four competitive channels of the 13DC reaction of pyrazinium-3-olate **1a** with MMA **5** are 6.9 (**TS1−6n**), 14.9 (**TS1−6x**), 11.8 (**TS1−2n**), and 18.5 (**TS1−2x**) kcal/mol. The most favorable reaction channel corresponds to the formation of [3 + 2] CA **9**, via **TS1−6n**. These energy results indicate that this 13DC is

dx.doi.org/10.1021/jo302730q | J. Org. Chem. 2013, 78, 1621−1629

Table 2. Relative Energies (in kcal/mol), in Gas Phase and in Acetonitrile, of the Stationary Points Involved in the Reaction of Pyrazinium-3-olate 1a with MMA 5

	gas phase	acetonitrile
TS1−6n	6.9	12.9
TS1−6x	14.9	15.9
TS1−2n	11.8	17.2
TS1−2x	18.5	21.3
9	−10.9	−2.0
10	−14.0	−5.5
11	−14.7	−6.1
12	−17.1	−8.2
TS2	6.5	10.0
6	0.2	0.1
TS3	11.3	30.0
13 + Cl^-	−8.1	16.8

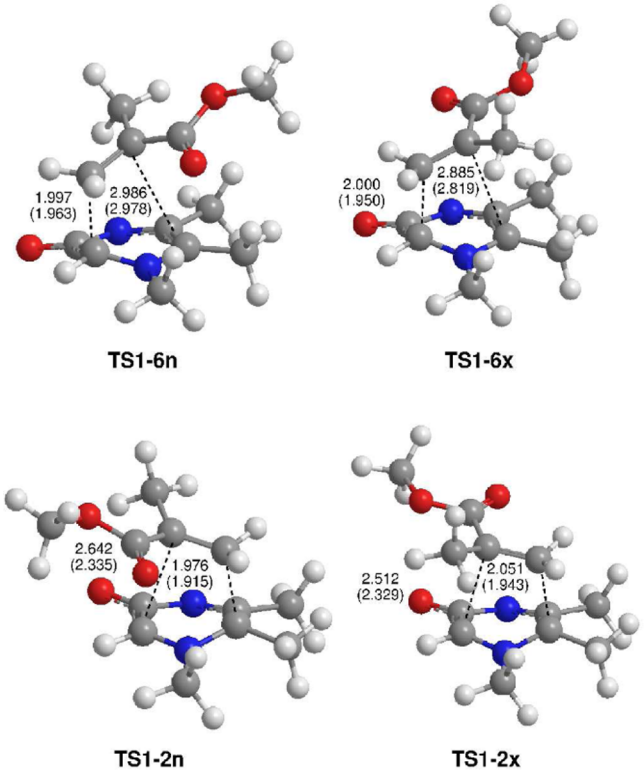

Figure 2. B3LYP/6-31G(d) transition structures for the 13DC reaction of pyrazinium-3-olate **1a** with MMA **5**. The values of the bond lengths directly involved in the processes are given in Å. The values corresponding to the reaction in acetonitrile are given in parentheses.

entirely *endo* stereoselective, **TS1−6x** being 8.0 kcal/mol higher in energy than **TS1−6n**, and completely 6 regioselective, **TS1−2n** being 4.9 kcal/mol higher in energy than **TS1−6n**. Formation of the CAs is exothermic, between −10.9 and −17.1 kcal/mol.

The geometries of the TSs involved in the 13DC reaction of pyrazinium-3-olate **1a** with MMA **5** are given in Figure 2. At the TSs associated with the regioisomeric channels *6*, the length of the C2−C1′ forming bonds are 1.997 Å at **TS1−6n** and 2.000 Å at **TS1−6x**, while the distance between the C6 and the C2′ atoms is 2.986 Å at **TS1−6n** and 2.885 Å at **TS1−6x**. At the TSs associated with the regioisomeric *channels 2*, the length of the C6−C1′ forming bonds are 1.976 Å at **TS1−2n** and 2.051 Å at **TS1−2x**, while the distance between the C2 and the C2′ atoms is 2.642 Å at **TS1−2n** and 2.512 Å at **TS1−2x**.

The extent of the asynchronicity of the bond-formation can be measured by the difference between the lengths of the two σ bonds being formed in the reaction, i.e., $\Delta d = d1 - d2$. The asynchronicity at the regioisomeric *channels 6* is Δd = 0.99 Å at **TS1−6n** and 0.88 Å at **TS1−6x**, while that at the regioisomeric *channels 2* is Δd = 0.67 Å at **TS1−2n** and 0.46 Å at **TS1−2x**. Formations of the most favorable TSs associated with *channels 6* are more asynchronous than those associated with *channels 2*. The IRCs from TSs to CAs clearly connect with the corresponding [3 + 2] CAs. At **TS1−6n** only the C2−C1′ σ bond is being formed by means of a favorable nucleophilic/electrophilic interaction between one of the most electrophilic centers of pyrazinium-3-olate **1a**, the C2 carbon, and the most electrophilic center of MMA **5**, the C1′ carbon.

Natural population analysis (NPA) allows us to evaluate the CT along this 13DC reaction path. The B3LYP/6-31G(d) natural atomic charges at the TSs were shared between the pyrazinium-3-olate **1a** and MMA **5**. At the TSs, the CT that fluxes from **1a** to MMA **5** is 0.12e at **TS1−6n**, 0.11e at **TS1−6x**, 0.16e at **TS1−2n**, and 0.12e at **TS1−2x**. These values indicate that these TSs have some zwitterionic character. The low CT found in this polar cycloaddition can be related to the low electrophilic character of MMA **5**; note that it is classified as a moderate electrophile.

As some of the species involved in the reaction between pyrazinium-3-olate **1a** and MMA **5** have a zwitterionic character, solvent effects in the reaction were considered by optimizing the gas phase geometries in acetonitrile. Inclusion of solvent effects increases the activation energies and decreases the exothermic character of the reactions as a consequence of a larger stabilization of the pyrazinium-3-olate **1a** when compared with the other species (see Table 2).[28] Solvent effects are different on the *endo* TSs, **TS1−6n** and **TS1−2n**, than on the *exo* ones, **TS1−6x** and **TS1−2x**. The latter two are more stabilized than the *endo* ones. In spite of this, formation of the *6-endo* [3 + 2] CA via **TS1−6n** remains the most favorable reaction channel. In acetonitrile the activation energy of the 13DC reaction rises to 12.9 kcal/mol, the reaction being exothermic by −2.0 kcal/mol.

Inclusion of solvent effects provokes minor changes in the geometries of the TSs associated with the regioisomeric *channels 6*. A different behavior is found at the TSs associated with the regioisomeric *channels 2*; along these channels, solvent effects decrease the asynchronicity of the bond formation since the length of the C2−C2′ forming bond is reduced to 2.335 Å at **TS1−2n** and 2.329 Å at **TS1−2x** (see Figure 2).

2.2. Conversion of [3 + 2] CA 9 into [4 + 2] CA 6. Conversion of [3.2.1] bicyclic structure **9** into [2.2.2] bicyclic structure **6** requires a skeletal rearrangement associated with a 1,2-carbon shift. An exploration of the PES associated with this isomerization made it possible to find one TS, **TS2**. In gas phase, the activation energy associated with this isomerization process via **TS2** is 17.4 kcal/mol (see Table 2). Although this activation energy is 6.9 kcal/mol higher than that associated with the 13DC reaction, **TS2** is positioned below **TS1−6n** because of the exothermic character of the formation of **9**. Formation of formal [4 + 2] CA **6** from [3 + 2] CA **9** is endothermic by 11.2 kcal/mol. However, the favorable thermochemistry associated with the formation of lactone−

dx.doi.org/10.1021/jo302730q | J. Org. Chem. 2013, 78, 1621−1629

lactam **8** may displace this unfavorable equilibrium toward formation of [2.2.2] bicyclic compound **6** (see below).

The gas phase geometry of **TS2** is given in Figure 3. The length of the C5−C2′ forming bond at **TS2** is 2.097 Å, while the distance between the C6 and the C2′ atoms is 2.568 Å. The length of the C2−C1′ bond at **TS2** is 1.577 Å. Analysis of the atomic movements at the unique imaginary frequency of **TS2** (−366.6 cm^{-1}) indicates that this TS is mainly associated with the C5−C2′ breaking bond. The IRCs from TS to reagent and product directly connect structure **9** with **6**.

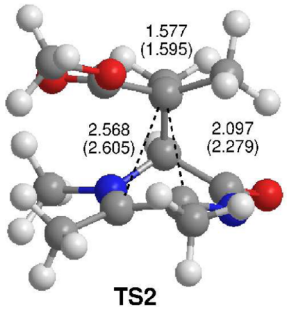

Figure 3. Transition structure **TS2** involved in the isomerization of [3 + 2] CA **9** into [4 + 2] CA **6**. The values of the bond lengths directly involved in the processes are given in Å. The values corresponding to the reaction in acetonitrile are given in parentheses.

In acetonitrile, the activation energy associated with this isomerization process via **TS2** is 12.0 kcal/mol. Formation of [4 + 2] CA **6** from **9** is endothermic by 1.9 kcal/mol. Consequently, solvent effects play an important role in the isomerization process; both the gas phase activation energy and the endothermic character are reduced by ca. 5 kcal/mol.

The geometry of **TS2** involved in the isomerization of **9** to **6** in acetonitrile is given in Figure 3. At **TS2**, the length of the C5−C2′ forming bond is 2.279 Å, while the distance between the C6 and C2′ atoms is 2.605 Å.

2.3. Formation of Lactone−Lactam 8. First, we investigated the formation of the zwitterionic intermediate **7**, which was proposed as an intermediate in the formation of lactone−lactam **8** (see Scheme 2). However, all attempts to locate **7** as a stationary point were unsuccessful, yielding formal [4 + 2] CA **6** (see Scheme 4). In addition, a scan of the reaction profile associated with the nucleophilic attack of the carboxyl oxygen on the iminium carbon showed that the relative gas phase energy of **6** rises to 28.7 kcal/mol. These results indicate that formation of **7** from **6** is kinetically and thermodynamically unfavorable. These results can be understood as a consequence of the poor nucleophilic character of the carboxylate group carbonyl oxygen present in **6**.

The carboxylate anion is a more powerful nucleophile, but its formation requires the elimination of the methyl group from the ester. Since this reaction is carried out experimentally in presence of iodide anion, this anion can provoke a nucleophilic attack on the carbon atom of the methyl group promoting a bimolecular nucleophilic S_N2 substitution to yield methyl iodide plus the corresponding carboxylate anion, which could then attack the iminium carbon.

To investigate this reaction path, we used chloride anion instead of iodide. In this way, **TS3** associated with the S_N2 reaction between chloride anion and the methyl carboxylate group of the formal [4 + 2] cycloadduct **6** was easily located, being, in gas phase, only 11.3 kcal/mol above **6** plus chloride anion (see Table 2). An analysis of the atomic movements at the unique imaginary frequency of **TS3** (−413.6 cm^{-1}) showed that it is mainly associated with the Cl−C bond formation and the C−O breaking bond process involved in the S_N2 reaction. However, the IRC from **TS3** to the product provides, in an elementary step, lactone−lactam enolate **13**, which in a slightly acidic medium, can yield the final lactone−lactam **8** (see Scheme 4). Reaction of **6** with chloride anion results in the formation of **13** and methyl chloride, which is exothermic by −8.1 kcal/mol.

The geometry of **TS3** is given in Figure 4. At **TS3** the lengths of the Cl−C forming bond and C−O breaking bond are 2.385 and 1.941 Å, respectively, while the distance between the carboxyl oxygen and the iminium carbon is 2.333 Å.

In acetonitrile, the activation energy associated with **TS3** rises to 30.0 kcal/mol, while formation of **13** plus methyl chloride turns endothermic to 16.8 kcal/mol. These unfavorable energies can be attributed to the strong solvation of chloride anion with the insertion of solvent effects.

Finally, all stationary points involved in the formation of lactone−lactam enolate **13** were optimized at the B3LYP/6-311G(d) level. The gas phase energies and TS geometries are given in Table S2 and Figure S1 in the Supporting Information.

Scheme 4. Formation of Lactone−Lactam 8

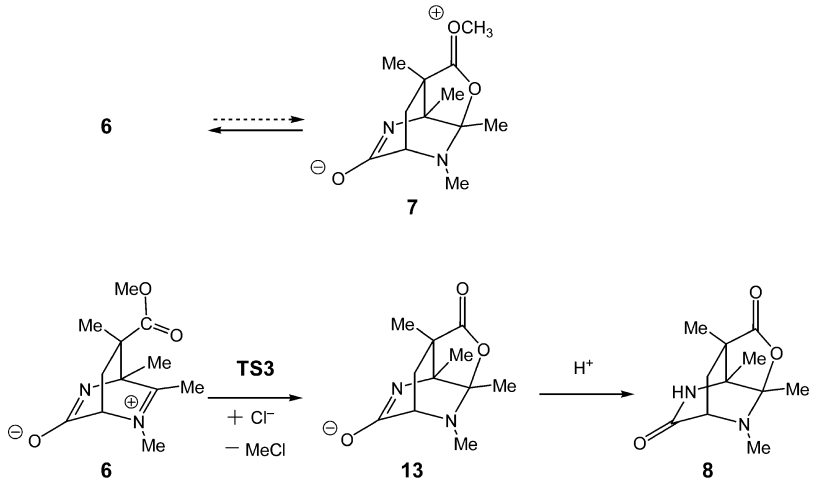

dx.doi.org/10.1021/jo302730q | J. Org. Chem. 2013, 78, 1621−1629

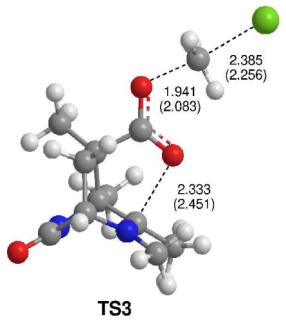

Figure 4. Transition structure **TS3** involved in the formation of the lactone ring. The values of the bond lengths directly involved in the processes are given in Å. The values corresponding to reaction in acetonitrile are given in parentheses.

A comparison of the gas phase relative energies using the two basis sets indicates that there are not significant changes. The gas phase activation energies associated with the three sequential steps increase only by 0.6−1.8 kcal/mol as a consequence of a larger stabilization of reagents than TSs. A similar trend is found in the solvent results. On the other hand, a comparison of the B3LYP/6-31G(d) geometries of **TS1−6n** and **TS2** and **TS3** given in Figures 2, 3, and 4 with the B3LYP/6-311G(d) TSs geometries given in Figure S1 (Supporting Information) also shows minor changes. Consequently, the use of triple-ζ functions does not improve the 6-31G(d) results.

3. ELF Bonding Analysis along the Formation of the Most Favorable [3 + 2] CA 9 and Its Isomerization into the Formal [4 + 2] CA 6. Several theoretical studies have shown that topological ELF analysis along a reaction path can be used as a valuable tool to understand the bonding changes along the path.[29−31] After an analysis of the electron density, the ELF provides basins, which are the domains in which the probability of finding an electron pair is maximal.[15e] The basins are classified as core basins and valence basins. The latter are characterized by the synaptic order, that is, the number of atomic valence shells in which they participate. Thus, there are monosynaptic, disynaptic, trisynaptic basins and so on.[15e] Monosynaptic basins, labeled V(A), correspond to the lone pairs or non-bonding regions, while disynaptic basins connect the core of two nuclei A and B and, thus, correspond to a bonding region between A and B and are labeled as V(A,B). This description recovers the Lewis bonding model, providing a very suggestive graphical representation of the molecular system.

In order to explain the forming and breaking bond processes along the 13DC reaction between pyrazinium-3-olate **1a** and

Table 3. Valence Basin Populations *N* Calculated from the ELF of Some Selected Points of the 13DC Reaction between Pyrazinium-3-olate 1a and MMA 5 and the Subsequent Isomerization of [3 + 2] CA 9 into [4 + 2] CA 6[a]

	1a	5	TS1−6n	P1−I	P2−I	9	P1−II	TS2	P2−II	6
*d*1(C2−C1′)			1.997	1.933	1.605	1.561	1.573	1.577	1.568	1.542
*d*2(C6−C2′)			2.986	2.969	2.409	1.643	1.961	2.568	2.535	2.503
*d*3(C5−C2′)			3.085	3.071	2.687	2.580	2.558	2.097	1.972	1.616
BO(C2−C1′)			0.48	0.55	0.90	0.96	0.95	0.93	0.95	0.98
BO(C6−C2′)			0.10	0.12	0.32	0.89	0.65	0.08	0.06	0.01
BO(C5−C2′)			0.05	0.06	0.08	0.01	0.04	0.45	0.57	0.86
V(N1,C2)	3.08		2.14	2.12	1.75	1.67	1.69	1.87	1.86	1.87
V(C2,C3)	2.98		2.33	2.31	2.18	2.16	2.16	2.1	2.08	2.03
V(C3,N4)	2.18		2.21	2.19	2.14	2.05	2.07	2.32	2.35	2.53
V(N4,C5)	2.62		2.64	2.65	2.67	2.88	2.83	2.14	1.94	1.64
V(C5,C6)	3.32		3.05	3.03	2.48	2.15	2.24	2.43	2.35	2.25
V(N1,C6)	2.41		2.55	2.55	2.40	1.74	1.9	2.98	3.06	3.84
V(C3,O7)	2.23		2.32	2.35	2.48	2.45	2.51	2.36	2.29	2.20
V(N1)			0.94	1.01	1.60	2.26	2.02	0.93	0.85	
V(N4)	2.81		2.84	2.83	2.90	2.75	2.81	3.22	3.34	3.45
V(C1′,C2′)		1.67	2.99	2.71	2.16	1.93	2.01	2.07	2.03	1.88
V′(C1′,C2′)		1.81								
V(C2′,C3′)		2.34	2.55	2.59	2.53	2.23	2.34	2.47	2.40	2.24
V(C6)					0.36		0.70			
V(C2′)				0.20	0.60		0.83	0.72		
V(C6,C2′)						1.86				
V(C5)								0.40		
V(C5,C2′)									1.34	1.86
V(C2)			0.60							
V(C1′)			0.30							
V(C2,C1′)				1.05	1.71	1.85	1.80	1.78	1.79	1.86

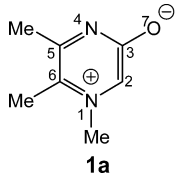

1a

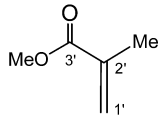

5

[a]The BO values[32] of the forming and breaking bonds are also included.

dx.doi.org/10.1021/jo302730q | J. Org. Chem. 2013, 78, 1621−1629

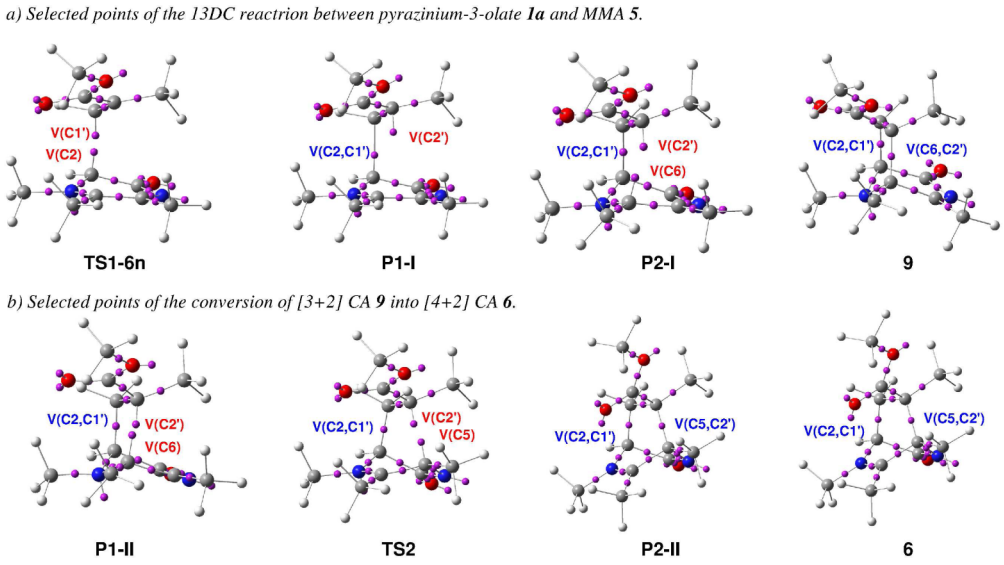

Figure 5. Attractor positions and atom numbering of some selected points of the 13DC reaction between pyrazinium-3-olate **1a** and MMA **5** and the subsequent isomerization of [3 + 2] CA **9** into [4 + 2] CA **6**.

MMA **5** and the subsequent isomerization of [3 + 2] CA **9** into [4 + 2] CA **6**, a topological ELF analysis along the IRCs of the two reaction paths was performed. The most relevant ELF valence basins and their corresponding *N* populations of the selected points along the two reaction paths are displayed in Table 3, while the attractor positions and atom numbering for some points are shown in Figure 5. For simplicity, only the monosynaptic V(A) and the disynaptic V(A,B) basins involved in the forming and breaking bonds will be discussed.

In pyrazinium-3-olate **1a**, the presence of one monosynaptic basin V(N4), integrating 2.81e, at the N4 nitrogen, and the absence of a monosynaptic basin at the N1 nitrogen as a consequence of its complete delocalization are the most noticeable features. Note that the population of the disynaptic basins V(N1,C2) and V(N1,C6) are 3.08e and 2.41e, respectively, as a consequence of this electron delocalization. In MMA **5**, the presence of two disynaptic basins V(C1′,C2′) and V′(C1′,C2′), integrating 1.67e and 1.81e, which are associated with the C1′−C2′ double bond, is the most noticeable feature. At **TS1−6n**, *d*1 = 1.997 Å and *d*2 = 2.986 Å, the two disynaptic basins V(C1′,C2′) and V′(C1′,C2′) present at MMA **5** have merged into the disynaptic basin V(C1′,C2′), which integrates 2.99e. The presence of two new monosynaptic basins, V(C2) and V(C1′), integrating 0.60e and 0.30e, respectively, is noteworthy. These monosynaptic basins are located at one of the most nucleophilic centers of pyrazinium-3-olate **1a**, and at the most electrophilic center of MMA **5**.[30,31] At point **P1−I**, *d*1 = 1.933 Å and *d*2 = 2.969 Å, the two monosynaptic basins V(C2) and V(C1′) present at **TS1−6n** have merged into the new disynaptic basin V(C2,C1′), which integrates 1.05e. This change indicates that the C2−C1′ bond formation has started at a C2−C1′ distance of 1.933 Å. At this point of the IRC, a new monosynaptic basin V(C2′) integrating 0.20e appears at the C2′ carbon of MMA **5**. At point **P2−I**, *d*1 = 1.605 Å and *d*2 = 2.409 Å, while the monosynaptic basin V(C2′) has reached 0.60e, a new monosynaptic basin V(C6) integrating 0.36e appears at the C6 carbon of pyrazinium-3-olate **1a**. Finally, at [3 + 2] CA **9**, *d*1 = 1.561 Å and *d*2 = 1.643 Å, while the two monosynaptic basins V(C6) and V(C2′) present at **P2−I** have merged into the new disynaptic basin V(C6,C2′) integrating 1.86e, the population of the disynaptic basin V(C2,C1′) has reached 1.85e.

Along the conversion of [3 + 2] CA **9** into [4 + 2] CA **6**, the first relevant point corresponds to **P1−II**, *d*2 = 1.961 Å and d3 = 2.558 Å, in which the disynaptic basin V(C6,C2′) created at the end of the 32CA reaction splits in two monosynaptic basins V(C6) and V(C2′), which integrate 0.70e and 0.83e, respectively. This behavior indicates that the C6−C2′ bond is already broken at this point. Along the reaction path associated with the isomerization process, the fluctuation of the electron density of the disynaptic basin V(C2,C1′) is below 0.07e. At **TS2**, *d*2 = 2.568 Å and d3 = 2.097 Å, while the monosynaptic basin V(C6) disappears, a new monosynaptic basin V(C5), integrating 0.40e appears at the C5 carbon. Therefore, while the C6−C2′ bond is already broken at **TS2**, the formation of the C5−C2′ bond has not started. This behavior allows us to characterize this isomerization as a non-concerted process. At point **P2−II**, *d*2 = 2.535 Å and *d*3 = 1.972 Å, the two monosynaptic basins V(C5) and V(C2′) have merged into the new disynaptic basin V(C5,C2′), which integrates 1.34e. This behavior indicates that at this point of the IRC, the C5−C2′ bond is already being formed. From this point to [4 + 2] CA **6**, the population of the disynaptic basin V(C5,C2′) increases to reach 1.86e.

Some interesting conclusions can be drawn from this ELF analysis: (i) ELF analysis of the 13DC reaction between pyrazinium-3-olate **1a** and MMA **5** indicates that formation of [3 + 2] CA **9** takes place via a two-stage mechanism,[33] in which the formation of the two σ bond takes place through a non-concerted process. While the C2−C1′ bond is formed in the first stage of the reaction, the formation of the second C6−C2′ bond takes place along the second stage; (ii) ELF analysis of the isomerization of [3 + 2] CA **9** into [4 + 2] CA **6** indicates that this process is also non-concerted; note that at **TS2** while the C6−C2′ bond is already broken, the C5−C2′ bond formation has not yet started; (iii) in spite of the electronic similarity between points **P2−I** and the **P1−II**, whose C6−C2′ bond is broken, they correspond to different reaction paths; (iv) ELF analysis of the IRCs associated with the two consecutive reactions asserts that [4 + 2] CA **6** cannot be

dx.doi.org/10.1021/jo302730q | J. Org. Chem. 2013, 78, 1621−1629

obtained in a direct way from pyrazinium-3-olate **1a** plus MMA **5**; and (v) as observed in previous 13DC and DA reactions, formation of C−C σ bonds takes place within a short-range of distances around 1.950 Å, in which two monosynaptic basins, V(Ca) and V(Cb), located at the two interacting carbons Ca and Cb, merge into a new disynaptic basin V(Ca,Cb) associated with the formation of the new Ca−Cb σ bond via a *pseudo-diradical* Ca-to-Cb coupling.[32]

CONCLUSIONS

The reaction between pyrazinium-3-olate **1a** and MMA **5** yielding lactone−lactam **8** has been studied using DFT methods at the B3LYP/6-31G(d) level. Formation of lactone−lactam **8** is a domino process involving three consecutive reactions: (i) a 13DC reaction between pyrazinium-3-olate **1a** and MMA **5** yielding [3 + 2] CA **9**; (ii) a skeletal rearrangement, which converts [3 + 2] CA **9** into formal [4 + 2] CA **6**, possessing a diazabicyclo[2.2.2]octane structure; and finally, (iii) an S_N2 reaction, promoted by halide anion, with concomitant nucleophilic attack of the carboxylate anion, thus created, on the iminium carbon with formation of the lactone ring present in **8**.

Energy analysis of the four competitive channels associated with the 13DC reaction between pyrazinium-3-olate **1a** and MMA **5** indicates that this cycloaddition takes place with a complete *endo* stereoselectivity and *6* regioselectivity, yielding [3 + 2] CA **9**, being the only CA that can experience this domino process. IRC analysis of the highly asynchronous **TS1−6n**, which is associated with the most favorable two-center nucleophilic/electrophilic interaction between the C6 carbon of the pyrazinium-3-olate ring of **1a** and the β conjugated position of MMA **5**, indicates that it is directly connected to the reagents and to the [3 + 2] CA **9**. The subsequent skeletal rearrangement also takes place in a single step via a non-concerted mechanism; in **TS2**, while the C6−C2′ bond is already broken, the C5−C2′ bond formation has not yet started.

This ELF bonding analysis makes it possible to establish that the diazabicyclo[2.2.2]octane skeleton present in the product **8** is not attained via a Diels−Alder reaction between pyrazinium-3-olate **1a** and MMA **5**, as was previously suggested for consideration.[7] In spite of the large electronic similarity found between points **P2−I** and the **P1−II**, in which the C2−C1′ σ bond is completely formed and the C6−C2′ and the C5−C2′ σ bonds are not still formed, they correspond to IRCs of two different reaction paths; while **P2−I** is located at the end of the 13DC reaction, **P1−II** is located at the beginning of the subsequent skeletal rearrangement. It also seems reasonable to extrapolate this result and conclude that the [3 + 2] CAs obtained from pyridinium-3-olates[5] are the results of direct 13DC reactions and do not involve the intervention of a [4 + 2] CA intermediate. A future publication will consider this aspect of the 13DCs of pyridinium-3-olates explicitly.

ASSOCIATED CONTENT

Supporting Information

Total energies, in gas phase and in acetonitrile, of the stationary points involved in the reaction of pyrazinium-3-olate **1a** with MMA **5**. B3LYP/6-311G(d) total and relative energies of the stationary points involved in the formation of lactone−lactam enolate **13**. B3LYP/6-311G(d) geometries of the TSs involved in the formation of lactone−lactam enolate **13**. B3LYP/6-31G(d) computed total energies, unique imaginary frequency, and Cartesian coordinates of the stationary points involved in the reaction of pyrazinium-3-olate **1a** with MMA **5**. This material is available free of charge via the Internet at http://pubs.acs.org.

AUTHOR INFORMATION

Corresponding Author

*E-mail: domingo@utopia.uv.es.

Notes

The authors declare no competing financial interest.

REFERENCES

(1) (a) Kumar, R. R.; Perumal, S. *Tetrahedron* **2007**, *63*, 7850−7857. (b) Kumar, R. R.; Perumal, S.; Manju, S. C.; Bhatt, P.; Yogeeswari, P.; Sriram, D. *Bioorg. Med. Chem. Lett.* **2009**, *19*, 3461−3465.

(2) (a) Desimoni, G.; Tacconi, G.; Barco, A.; Pollini, G. P. *Natural Products Synthesis through Pericyclic Reactions*; American Chemical Society: Washington, D.C., 1983. (b) Padwa, A. In *Synthetic Applications of 1,3-Dipolar Cycloaddition Chemistry toward Heterocycles and Natural Products*; Wiley: Hoboken, NJ, 2003. (c) Merino, P. In *Science of Synthesis*; Padwa, A., Ed.; George Thieme: New York, NY, 2004; Vol. *27*, p 511.

(3) (a) Massiot, G.; Delaude, C. *Alkaloids* **1986**, *27*, 300−321. (b) Plunkett, A. O. *Nat. Prod. Rep.* **1994**, *11*, 581−590. (c) Chorghade, M. S.; Cseke, C. *Pure Appl. Chem.* **1994**, *66*, 2211−2214. (d) Feng, G.-L.; Zhang, H.-L.; Geng, L.-J. *J. Chem. Res.* **2011**, *35*, 121−123.

(4) (a) Kaval, N.; Ermolat'ev, D.; Appukkuttan, P.; Dehaen, W.; Kappe, C. O.; Van der Eycken, E. *J. Comb. Chem.* **2005**, *7*, 490−502. (b) Pawar, V. G.; De Borggraeve, W. M. *Synthesis* **2006**, 2799−2814. (c) Samori, C.; Ali-Boucetta, H.; Sainz, R.; Guo, C.; Toma, F. M.; Fabbro, C.; da Ros, T.; Prato, M.; Kostarelos, K.; Bianco, A. *Chem. Commun.* **2010**, *46*, 1494−1496. (d) Hashimoto, T.; Maeda, Y.; Omote, M.; Nakatsu, H.; Maruoka, K. *J. Am. Chem. Soc.* **2010**, *132*, 4076−4077.

(5) (a) Katritzky, A. R.; Takeuchi, Y. *J. Chem. Soc. C* **1971**, 874−877. (b) Dennis, N.; Katritzky, A. R.; Matsuo, T.; Parton, S. K.; Takeuchi, Y. *J. Chem. Soc., Perkin Trans. 1* **1974**, 746−750. (c) Banerji, J.; Dennis, N.; Frank, J.; Katritzky, A. R.; Matsuo, T. *J. Chem. Soc., Perkin Trans. 1* **1976**, 2334−2338. (d) Dennis, N.; Katritzky, A. R.; Takeuchi, Y. *Angew. Chem., Int. Ed. Engl.* **1976**, *15*, 1−9.

(6) (a) Allway, P. A.; Sutherland, J. K.; Joule, J. A. *Tetrahedron Lett.* **1990**, *31*, 4781−4783. (b) Yates, N. D.; Peters, D. A.; Allway, P. A.; Beddoes, R. L.; Scopes, D. I. C.; Joule, J. A. *Heterocycles* **1995**, *40*, 331−347. (c) Helliwell, M.; You, Y.; Joule, J. A. *Heterocycles* **2006**, *70*, 87−91. (d) Helliwell, M.; You, Y.; Joule, J. A. *Acta Crystallogr., Sect. E: Struct. Rep. Online* **2006**, *62*, o1293−o1294. (e) Helliwell, M.; You, Y.; Joule, J. A. *Acta Crystallogr., Sect. E: Struct. Rep. Online* **2006**, *62*, o2318−o2320. (f) Kiss, M.; Russell-Maynard, J.; Joule, J. A. *Tetrahedron Lett.* **1987**, *28*, 2187−2190.

(7) Joomun, Z.; Raftery, J.; Delawarally, K.; Laulloo, S. J.; Joule, J. A. *ARKIVOC* **2007**, *(xvi)*, 51−77.

(8) Rhyman, L.; Abdallah, H. H.; Jhaumeer-Laulloo, S.; Domingo, L. R.; Joule, J. A.; Ramasami, P. *Curr. Org. Chem.* **2012**, *16*, 1711−1722 and references cited therein.

(9) (a) Lee, C.; Yang, W.; Parr, R. G. *Phys. Rev. B* **1988**, *37*, 785−789. (b) Becke, A. D. *J. Chem. Phys.* **1993**, *98*, 5648−5652.

(10) Hehre, W. J.; Radom, L.; Schleyer, P. v. R.; Pople, J. A. *Ab Initio Molecular Orbital Theory*; Wiley: New York, 1986.

(11) (a) Schlegel, H. B. *J. Comput. Chem.* **1982**, *2*, 214−218. (b) Schlegel, H. B. In *Modern Electronic Structure Theory*; Yarkony, D. R., Ed.; World Scientific Publishing: Singapore, 1994.

(12) Fukui, K. *J. Phys. Chem.* **1970**, *74*, 4161−4163.

(13) (a) González, C.; Schlegel, H. B. *J. Phys. Chem.* **1990**, *94*, 5523−5527. (b) González, C.; Schlegel, H. B. *J. Chem. Phys.* **1991**, *95*, 5853−5867.

(14) (a) Reed, A. E.; Weinstock, R. B.; Weinhold, F. *J. Chem. Phys.* **1985**, *83*, 735−746. (b) Reed, A. E.; Curtiss, L. A.; Weinhold, F. *Chem. Rev.* **1988**, *88*, 899−926.
(15) (a) Savin, A.; Becke, A. D.; Flad, J.; Nesper, R.; Preuss, H.; von Schnering, H. G. *Angew. Chem., Int. Ed.* **1991**, *30*, 409−412. (b) Silvi, B.; Savin, A. *Nature* **1994**, *371*, 683−686. (c) Savin, A.; Silvi, B.; Colonna, F. *Can. J. Chem.* **1996**, *74*, 1088−1096. (d) Savin, A.; Nesper, R.; Wengert, S.; Fassler, T. F. *Angew. Chem., Int. Ed. Engl.* **1997**, *36*, 1808−1832. (e) Silvi, B. *J. Mol. Struct.* **2002**, *614*, 3−10.
(16) Noury, S.; Krokidis, X.; Fuster, F.; Silvi, B. *Comput. Chem.* **1999**, *23*, 597−604.
(17) Frisch, M. J.; Trucks, G. W.; Schlegel, H. B.; Scuseria, G. E.; Robb, M. A.; Cheeseman, J. R.; Scalmani, G.; Barone, V.; Mennucci, B.; Petersson, G. A.; Nakatsuji, H.; Caricato, M.; Li, X.; Hratchian, H. P.; Izmaylov, A. F.; Bloino, J.; Zheng, G.; Sonnenberg, J. L.; Hada, M.; Ehara, M.; Toyota, K.; Fukuda, R.; Hasegawa, J.; Ishida, M.; Nakajima, T.; Honda, Y.; Kitao, O.; Nakai, H.; Vreven, T.; Montgomery, J. A.; Peralta, Jr., J. E.; Ogliaro, F.; Bearpark, M.; Heyd, J. J.; Brothers, E.; Kudin, K. N.; Staroverov, V. N.; Kobayashi, R.; Normand, J. ; Raghavachari, K.; Rendell, A.; Burant, J. C.; Iyengar, S. S.; Tomasi, J.; Cossi, M.; Rega, N.; Millam, J. M.; Klene, M.; Knox, J. E.; Cross, J. B.; Bakken, V.; Adamo, C.; Jaramillo, J.; Gomperts, R.; Stratmann, R. E.; Yazyev, O. ; Austin, A. J.; Cammi, R.; Pomelli, C.; Ochterski, J. W.; Martin, R. L.; Morokuma, K.; Zakrzewski, V. G.; Voth, G. A.; Salvador, P.; Dannenberg, J. J.; Dapprich, S.; Daniels, A. D. Farkas, J.; Foresman, B.; Ortiz, J. V.; Cioslowski, J.; Fox, D. J. *Gaussian 09*, Revision A.02; Gaussian, Inc.: Wallingford, CT, 2009.
(18) Parr, R. G.; von Szentpaly, L.; Liu, S. *J. Am. Chem. Soc.* **1999**, *121*, 1922−1924.
(19) (a) Parr, R. G.; Pearson, R. G. *J. Am. Chem. Soc.* **1983**, *105*, 7512−7516. (b) Parr, R. G.; Yang, W. *Density Functional Theory of Atoms and Molecules*; Oxford University Press: New York, 1989.
(20) Domingo, L. R.; Pérez, P. *Org. Biomol. Chem.* **2011**, *9*, 7168−7175 and references cited therein.
(21) Kohn, W.; Sham, L. J. *Phys. Rev.* **1965**, *140*, 1133−1338.
(22) Domingo, L. R.; Aurell, M. J.; Pérez, P.; Contreras, R. *J. Phys. Chem. A* **2002**, *106*, 6871−6875.
(23) Pérez, P.; Domingo, L. R.; Duque-Noreña, M.; Chamorro, E. *J. Mol. Struct.: THEOCHEM* **2009**, *895*, 86−91.
(24) Domingo, L. R.; Perez, P.; Sáez, J. A. *RSC Adv.* **2013**, *3*, 1486−1494.
(25) (a) Geerlings, P.; De Proft, F.; Langenaeker, W. *Chem. Rev.* **2003**, *103*, 1793−1784. (b) Ess, D. H.; Jones, G. O.; Houk, K. N. *Adv. Synth. Catal.* **2006**, *348*, 2337−2361.
(26) Domingo, L. R.; Aurell, M. J.; Pérez, P.; Contreras, R. *Tetrahedron* **2002**, *58*, 4417−4423.
(27) Jaramillo, P.; Domingo, L. R.; Chamorro, E.; Pérez, P. *J. Mol. Struct.: THEOCHEM* **2008**, *865*, 68−76.
(28) Benchouk, W.; Mekelleche, S. M.; Silvi, B.; Aurell, M. J.; Domingo, L. R. *J. Phys. Org. Chem.* **2011**, *24*, 611−618.
(29) (a) Berski, S.; Andres, J.; Silvi, B.; Domingo, L. R. *J. Phys. Chem. A* **2003**, *107*, 6014−6024. (b) Polo, V.; Andres, J.; Castillo, R.; Berski, S.; Silvi, B. *Chem.—Eur. J.* **2004**, *10*, 5165−5172. (c) Domingo, L. R.; Sáez, J. A. *J. Org. Chem.* **2011**, *76*, 373−379 and references cited therein.
(30) Rhyman, L.; Ramasami, P.; Joule, J. A.; Sáez, J. A.; Domingo, L. R. *RSC Adv.* **2013**, *3*, 447−457 and references cited therein.
(31) Domingo, L. R.; Pérez, P.; Sáez, J. A. *Tetrahedron* **2013**, *69*, 107−114 and references cited therein.
(32) Wiberg, K. B. *Tetrahedron* **1968**, *24*, 1083−1096.
(33) Domingo, L. R.; Sáez, J. A.; Zaragozá, J. R.; Arnó, M. *J. Org. Chem.* **2008**, *73*, 8791−8799.